water

MDPI

Article

Seasonality of Water Exchange in the Northern South China Sea from Hydrodynamic Perspective

Lingbo Cui [1], Mingyu Li [1], Tingting Zu [2,*] and Zhongya Cai [1,3,*]

[1] State Key Laboratory of Internet of Thing for Smart City, Department of Ocean Science and Technology, University of Macau, Macau 999078, China
[2] State Key Laboratory of Tropical Oceanography, South China Sea Institute of Oceanology, Chinese Academy of Sciences, Guangzhou 510301, China
[3] Center for Ocean Research in Hong Kong and Macau (CORE), Hong Kong 999077, China
* Correspondence: author: zutt@scsio.ac.cn (T.Z.); zycai@um.edu.mo (Z.C.)

Abstract: In this study, we utilized exposure time ($\overline{\theta}$) as a key metric to investigate water exchange and its spatiotemporal variations in the Northern South China Sea (NSCS). The Eulerian adjoint method and Lagrangian tracking were adopted to capture a comprehensive view of water exchange in coastal regions. Our findings reveal distinct spatial and seasonal variations in $\overline{\theta}$. Spatially, a long $\overline{\theta}$ (exceeding 150 days) appears in the coastal region, and the largest values occur in the Beibu Gulf (300 days). Temporally, $\overline{\theta}$ exhibits clear seasonal patterns across the extensive shelf area, influenced by the seasonal monsoon which induced seasonally reversing shelf current and results in symmetrical distribution patterns of $\overline{\theta}$ across the board shelf during both winter and summer months. $\overline{\theta}$ is longer in winter than in summer. The study also revealed pronounced vertical contrasts in cross-isobath transport over the NSCS shelf, though significant vertical variations in net exchange time were noted only in specific locations, including the northeast side of Hainan Island, the Beibu Gulf mouth, and along the west side of Taiwan Island. The Beibu Gulf emerged as a critical factor in the NSCS's water exchange dynamics in both seasons. In summer, it impacts more than 20% of the water exchange over adjacent areas, particularly through its westward transport against typical northeastward shelf currents. This highlights the combined effect of the westward spread of the Pearl River freshwater and the stable slope current on regional hydrodynamics. In winter, the Gulf's retention characteristics profoundly affected even distant areas, contributing to up to 50% of water exchange, showing its broad impact on the NSCS's water dynamics throughout the year.

Keywords: exposure time; Northern South China Sea; lagrangian and eulerian methods; seasonality; hydrodynamics

Citation: Cui, L.; Li, M.; Zu, T.; Cai, Z. Seasonality of Water Exchange in the Northern South China Sea from Hydrodynamic Perspective. *Water* **2024**, *16*, 10. https://doi.org/10.3390/w16010010

Academic Editor: Wencheng Guo

Received: 11 November 2023
Revised: 3 December 2023
Accepted: 11 December 2023
Published: 20 December 2023

1. Introduction

Coastal waters serve as critical interfaces where terrestrial and marine ecosystems intersect, playing an essential role in global material cycles. These waters, influenced by the confluence of rivers and oceans, are subject to dynamic processes shaped by tides, winds, buoyancy waters and ocean circulation [1–4]). Meanwhile, the functioning of coastal ecosystems is increasingly threatened by anthropogenic impacts and climate change, leading to detrimental effects such as eutrophication, harmful algal blooms, and hypoxia exacerbated by inadequate water exchange [5,6]. These ecological disturbances highlight the importance of understanding water exchange processes, as they are fundamental in determining the transport and fate of water quality indicators [7,8].

Over the Northern South China Sea (NSCS), the shelf circulation and water movement experience complex dynamics driven by wind, tides, the Kuroshio intrusion, freshwater discharge from the Pearl River Estuary (PRE), and modulated by the local topography [9,10]. The alternate variation of northeasterly winter monsoon to southwesterly summer monsoon induces contrasting seasonally changed southwestward to northeastward shelf current and

a strong seasonal difference in rainfall over southern China and related buoyant discharge into the NSCS, which together impacts water exchange rates and thus the ecological balance of the region [11,12]. Under the interaction of topography and summer southwesterly wind, extensive upwelling was generated at the coastal region of NSCS and brings cold, salty, nutrient-rich deep waters to the surface and therefore, improves the primary production in these regions [9,13,14]. Although previous studies have recognized the influence of the East Asia Monsoon on the NSCS's hydrodynamic processes, indicating substantial seasonal variability [15–17], the specific seasonal patterns of water exchange, the major hydrodynamic processes, and their cumulative impacts remain poorly understood.

Transport timescales and water exchange rates, crucial for evaluating the distribution of properties critical to marine ecosystems and climate, are significantly affected by seasonality of the seasonally contrasting shelf current. Metrics such as exposure time, water age, and flushing time, offer a high-resolution understanding of these variations and have proven effective for assessing coastal water exchange capacities, particularly in tidal regions where water reentry is a key factor [1,18]. These timescales are vital benchmarks in complex dynamic settings and provide insight into how varying conditions impact the transport of phytoplankton biomass and contaminants [19–22]. Earlier research on water exchange in the NSCS primarily concentrated on coastal regions, specifically estuarine areas, for instance, Ren et al. (2014) [23] found riverine influence plays a crucial role in water exchange in the Pearl River Estuary, with tides affecting the fluctuation range of water exchange. Wind predominantly impacts the vertical structure of water exchange during winter [24]. It is also noticed that the large-scale coastal controls the seasonal pattern of bay-shelf exchanges [25]. Over the shelf, research mainly focuses on the cross isobath water motions, such as Liu et al.'s [26] study highlighted that southwesterly wind induced flows in the Taiwan Strait sustained northeastward upwelling currents near the Pearl River Estuary, promoting the extensive upslope movement of deep shelf waters. Therefore, investigation into the seasonal patterns of water exchange in the NSCS and the related hydrodynamic processes could provide valuable information for the effective management and improvement of coastal environments, emphasizing the critical nature of seasonal dynamics in coastal water that is influenced by monsoon.

Following this introduction, Section 2 introduces the numerical model, adjoint model, and tracking model used in this study. Section 3 discusses the spatial-temporal characteristics of water exchange. Finally, Section 4 summarizes the study.

2. Methodology

2.1. Ocean Model

To accurately simulate estuarine and shelf circulation with high resolution, this study utilized a hierarchically nested modeling approach based on the Regional Ocean Modeling System [27]. The model's domain encompasses the NSCS shelf (Figure 1), with horizontal grid spacing that finely transitions from approximately 1 km in the coastal proximity to 3 km across the broader NSCS shelf area. Employing the terrain-following s-coordinate system [28], the vertical structure of the water column was discretized into 60 levels to enhance resolution and a higher resolution was used in both the surface and bottom boundary layers. To solve the turbulent mixing and diffusion in the water column, we utilized the level-2.5 turbulence-closure scheme of Mellor and Yamada (1982) [29]. The model incorporates atmospheric forcing including wind, heat flux, and precipitation, provided by the ERA5 atmospheric reanalysis data from the European Center for Medium-Range Weather Forecasts (ECMWF). River discharge data were provided by the Ministry of Water Resources of China. Along the open boundary, the model was nested with the Hybrid Coordinate Ocean Model and the Navy Coupled Ocean Data Assimilation (HYCOM + NCODA) global 1/12° analysis (GLBv0.08; https://www.hycom.org/), with a 3-hourly temporal interval. We imposed nine major constituents of the semidiurnal (i.e., M_2, S_2, K_2, and N_2) and diurnal (i.e., K_1, O_1, P_1, and Q_1) tides, as well as one of the M_4 tide from the nonlinearity of the M_2. These harmonic constants were inverted from remotely sensed

long-term sea-level anomaly (SLA) variations using the Oregon Tide Inverse Software (Egbert & Erofeeva, 2002; https://www.tpxo.net/otps) [30] of T. T. Zu et al. (2008) [31]. This modeling system has been previously validated for its efficacy in exploring climate influences and the interannual variability of shelf currents in the NSCS [32]. In this study, the daily results of velocity (u, v, w) and the diffusion coefficient (k) between 1994–2018 were saved to conduct the adjoint simulation under complex hydrodynamic conditions, detailed in the following contents.

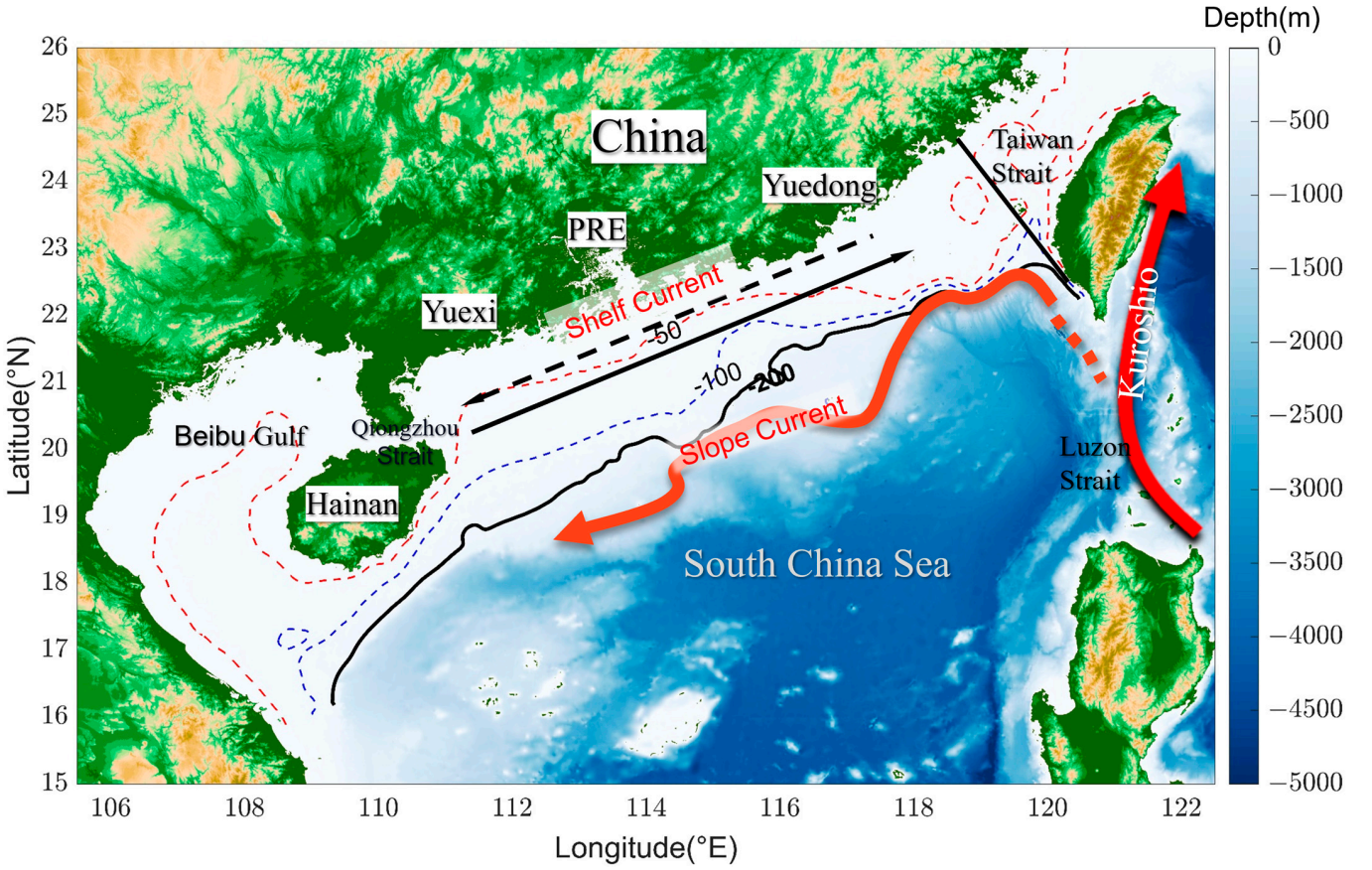

Figure 1. Topography (m) and diagrammatic sketch of circulation in the NSCS. The black solid/dashed arrow over the shelf indicates the summer/winter current. The black solid lines and 200 m isobath define the region of ω in the calculation of exposure time.

2.2. Exposure Time Model and Lagrangian Particle Tracking

To examine the water exchange capacity, the exposure time $(\overline{\theta})$ [33], which was defined as the time required for the released substance to leave the domain of interest (ω) was used as it showed high-resolution temporal and spatial variations. To resolve the dependence of $\overline{\theta}$ on the initial release location and release time, the adjoint method [34,35] was used.

$$\frac{\partial \overline{\theta}}{\partial t} + \delta_\omega + \vec{v} \cdot \nabla \overline{\theta} + \nabla \left(k \cdot \nabla \overline{\theta} \right) = 0 \tag{1}$$

where $\overline{\theta}$ is the exposure time, $\vec{v}$ is the three-dimensional velocity vector and k is the turbulent diffusion coefficient obtained from the hydrodynamic model, and δ_ω is the characteristic function of the domain of interest ω that $\delta_\omega = \begin{cases} 1 \ (x, y, z) \in \omega \\ 0 \ (x, y, z) \notin \omega \end{cases}$.

In this study, ω covers the region from Beibu Gulf to the Taiwan Strait. It is bounded by the 200-m isobath (Figure 1). In this study, the saved daily results of velocity (u, v, w) and the diffusion coefficient (k) were used to calculate the $\overline{\theta}$ offline. In the calculation, the initial value of $\overline{\theta}$ is set to zero in the computational domain and it was integrated backward

in time (from the present to the past) with the reversed flow [35,36]. Along the boundary of simulation domain, the $\overline{\theta}$ was set as zero, which indicates that after leaving the simulation domain, the water does not come back.

Besides using the $\overline{\theta}$, to reveal the transport pattern, the Lagrangian TRANSport model (LTRANS v.2b), which is a popular off-line three-dimensional particle tracking module [37–39] was used to track the motion of water parcels in a Lagrangian manner to identify the areas where water parcels gather. The fourth-order Runge–Kutta scheme was applied for particle advection and reflective boundary conditions were used to treat the particles that hit the solid boundaries. The effects of vertical and horizontal turbulence are considered by the random displacement model using the diffusivity coefficient from the hydrodynamic simulation [40,41]. Particles were released on each computational grid every 5 days during the simulation.

3. Results and Discussion

3.1. Shelf Circulation

In order to gain a comprehensive understanding of the hydrodynamic factors influencing water exchanges, we first examined the circulation patterns within the computational domain, focusing on climatologically averaged conditions for the distinct periods of summer and winter (Figure 2). The hydrodynamic variations between these seasons are pivotal for interpreting the mechanisms driving water exchange.

The circulation patterns in the NSCS shelf exhibit marked seasonal variations, closely linked to monsoonal influences and regional geomorphological features (Figure 2), meanwhile the Kuroshio intrusion through the Luzon Strait fosters a cyclonic slope current that serves as the dynamic boundary delineating the shelf circulation [42]. During the summer, the shelf current is directed northeastward under the influences of the southwesterly monsoon. Along the Yuexi coast that to the west of PRE, the northwestward coastal current to the west of PRE was largely reduced under the influence of the westward expanded plume from PRE. The river plume that comes from the PRE is mainly affected by the winds that drive currents along the coast. Additionally, the natural buoyancy within the plume plays a crucial role in altering the circulation of water both along the shore and across the shelf, especially in the upper layers of the water column. At the estuary mouth, the interaction of Pearl River Plume and shelf current induced the intrusion of shelf current [43,44]. It is also noticed that, during summer, the cyclonic slope current intruded into the shelf through the region to the southeast of Hainan Island and joined the shelf current (Figure 2a). On the surface, the complicated cross-isobath transport patterns occur around Hainan Island, but the bottom onshore intrusion prevails over the shelf due to the flow-topography interaction [10,45] (Figure 2c,d). Conversely, during winter, the shelf current intensifies and assumes a southwestward flow. Associated with the intensified northeast wind, the surface water mainly features the onshore intrusion, while the strong bottom offshore transport covers the whole shelf (Figure 2e,f), particularly to the southeast of Hainan Island. The cross-shelf velocities are instrumental in establishing the dynamic connection between the shelf current and the basin-wide circulation [26,46], and these velocities, combined with the observed seasonal circulation patterns, emphasize the complex interplay between shelf and basin dynamics in the region.

The Beibu Gulf, linked to the broader shelf via the Qiongzhou Strait, presents a less clear picture. The majority of evidence suggests a predominance of cyclonic and anticyclonic gyres controlling the circulation within the gulf [47,48]. However, during summer, currents weaken considerably, leading to a reduced water exchange capacity within the Beibu Gulf, contrasting with the well-defined gyres of winter. The complexity of these seasonal circulation patterns underscores the need for nuanced understanding when considering hydrodynamic impacts on water exchanges in the NSCS.

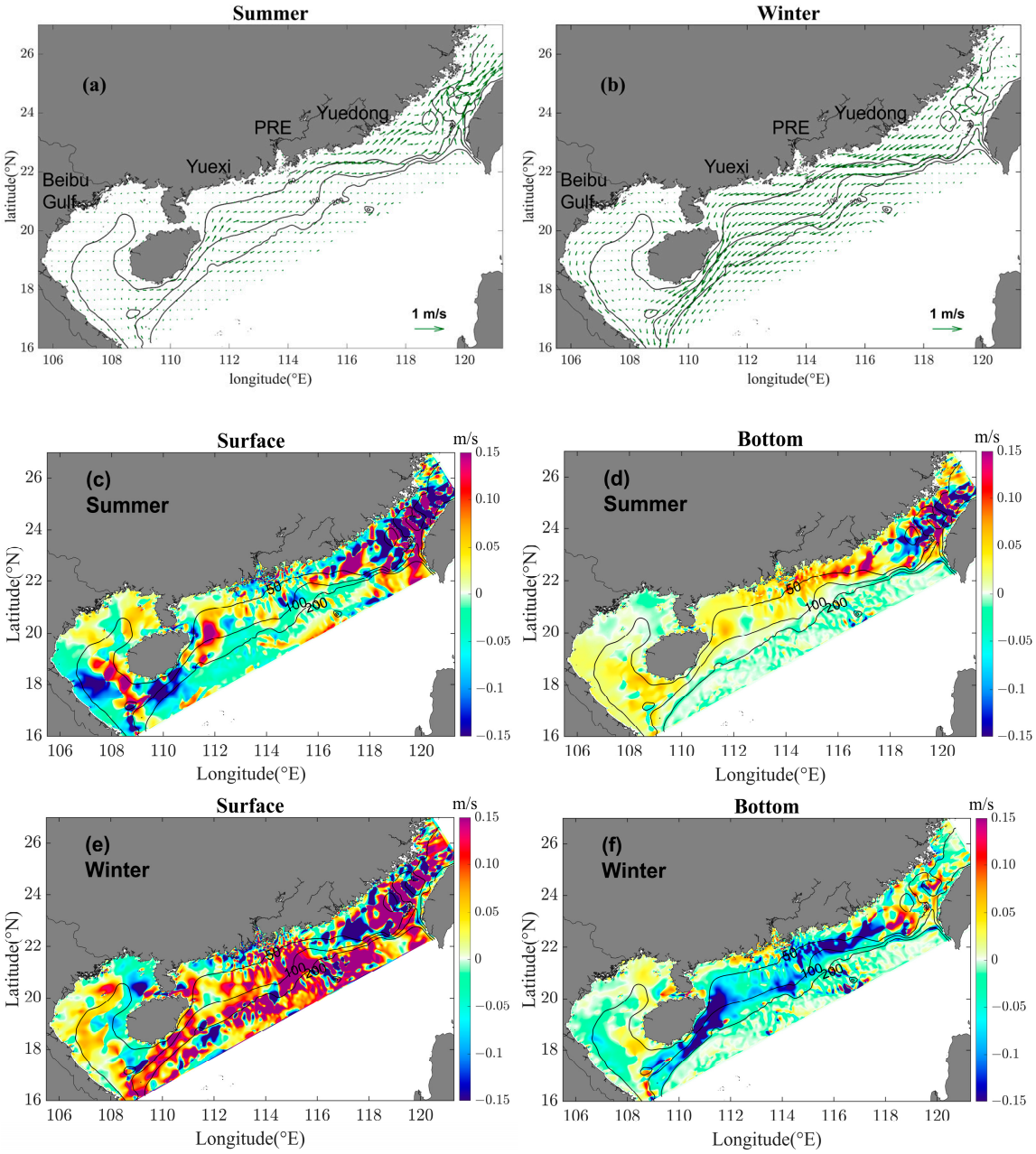

Figure 2. (**a**) Horizontal map of the depth-averaged shelf current in summer. (**b**) Same as (**a**), but for winter. (**c**,**d**) Summer cross isobath velocity (m/s) in surface and bottom, respectively, positive and negative values indicate the onshore and offshore motions, respectively. (**e**,**f**) Same as (**c**,**d**) but for winter.

3.2. Seasonal Variability of the $\overline{\theta}$

The Figure 3a depicts the spatial pattern of the annual mean $\overline{\theta}$ in the NSCS. Generally, the longest $\overline{\theta}$ with the magnitude of ~300 days is observed in the nearshore areas of the Beibu Gulf and the Yuexi shelf, where the circulation is relatively weaker (Figure 2a,b). Then it gradually decreases towards the outer shelf which correlates inversely with water depth and decreases northeastwardly from Beibu Gulf towards the Yuedong regions. In order to comprehensively examine the variability of $\overline{\theta}$, we conducted an Empirical Orthogonal Function (EOF) analysis. The dominant mode (Figure 3b), referred to as EOF-01, emerges as particularly significant, accounting for a substantial portion (47.5%) of the overall variance. In contrast, the subsequent modes each make relatively modest contributions, with each of them accounting for less than 15% of the total variance.

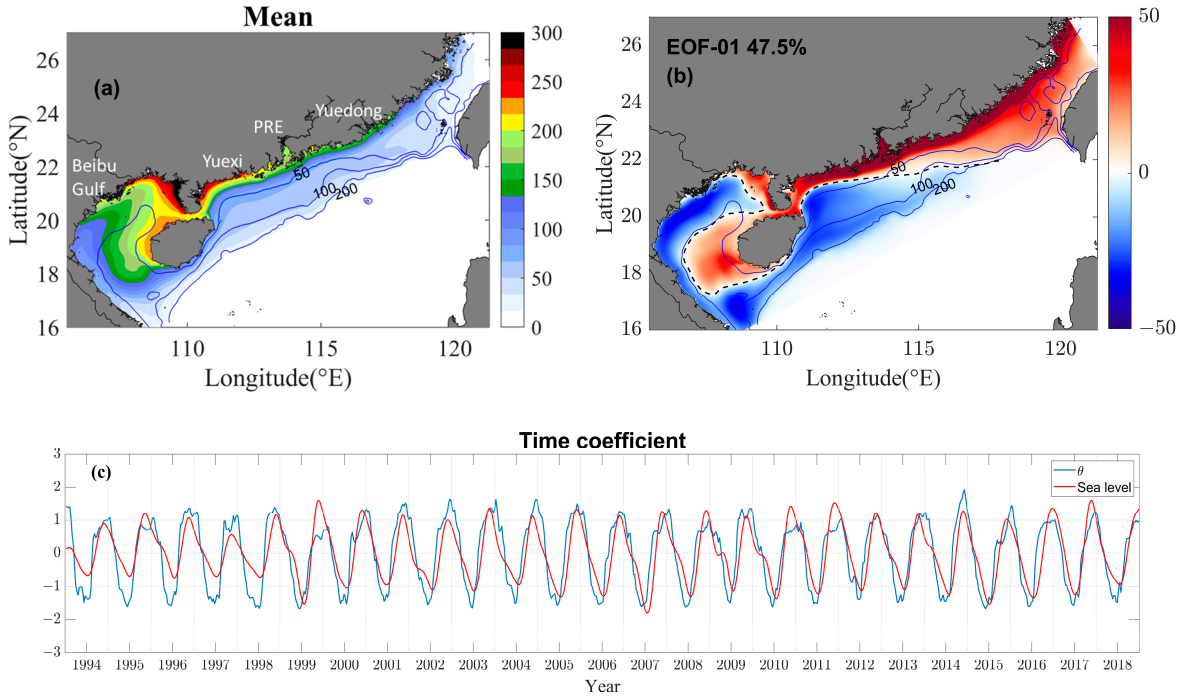

Figure 3. (**a**) The annual mean distribution of the depth-averaged $\overline{\theta}$ in NSCS. (**b**) EOF leading mode of $\overline{\theta}$. (**c**) Time coefficient of the leading mode of $\overline{\theta}$ and time coefficient of the leading mode of sea level.

The magnitude of $\overline{\theta}$ anomalies exhibit an increasing trend, transitioning from the outer shelf towards the inner shelf and coastal areas, particularly in the Beibu Gulf. It is also noted that a positive anomaly appears in the northeast corner of the Beibu Gulf, mirroring the anomaly observed in the coastal region of the shelf. This suggests a potential connection of circulations between the Beibu Gulf and the broader shelf region. Temporally, the time coefficient associated with EOF-01 exhibits clear seasonal fluctuations on an annual scale (Figure 3c). Compared with the time coefficient of the EOF-01 of sea level in NSCS, there is minimal time lag, indicating an almost immediate response of the water exchange rate to the hydrodynamic conditions. Seasonal variations in $\overline{\theta}$ are marked by lower values during the summer, in line with decreased sea levels, and higher values during the winter, corresponding with elevated sea levels.

To check the seasonality of the $\overline{\theta}$ in the NSCS, it was averaged in the summer and winter time during the simulation period. During the summer months, the robust northeastward shelf current initiates an active water exchange (Figure 2a), the substance released in the northeast shelf can leave the NSCS rapidly through the Taiwan Strait, thus diminishing $\overline{\theta}$ values along the northeast shelf. From the Taiwan Strait, there is a notable southwestward increase to approximately 200 days near Qiongzhou Strait (Figure 4a). The Beibu Gulf experiences complex interactions between anti-cyclonic circulation in its southern reaches and cyclonic circulation in the north (Figure 2a), causing $\overline{\theta}$ values to rise from the mouth of the bay toward the gulf's northeast and reach the largest exceeding 300 days. Meanwhile, the water motion is relatively weak, and induces the larger values $\overline{\theta}$ at the top of the Beibu Gulf.

In contrast, during winter, the distribution of $\overline{\theta}$ exhibits roughly opposite patterns (Figure 4b). The southwestward coastal current carries water into the Beibu Gulf via the Qiongzhou Strait (Figure 2b), resulting in a zonal distribution along the coastline of Guangdong Province. In the Beibu Gulf, a gulf-scale cyclonic circulation that is nested with a cyclonic gyre in the southern gulf emerges in winter [49]. The southwestward shelf current formed a strong jet at the southeast of Hainan Island and flow westward, then, it enters the Beibu gulf from the southwest side of Hainan Island and exits through the southern coastal region of Vietnam (Figure 2b), consequently, this circulation leads to low values of $\overline{\theta}$

along the eastern coast of Vietnam. Furthermore, the gulf-scale cyclonic gyre, extending northeastward, facilitates the transport of substances released in the northwest coast region of Hainan Island to the northern Gulf, where they may persist for an extended period.

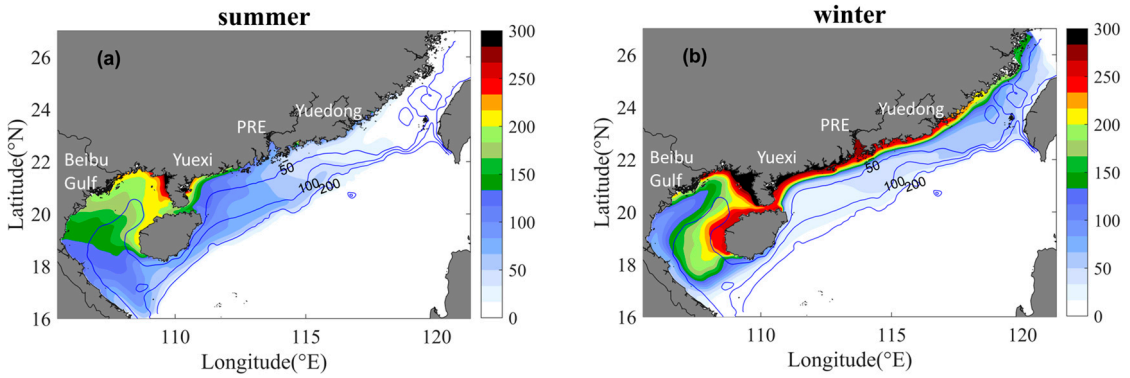

Figure 4. (**a**) Depth averaged exposure time in summer ($\bar{\theta}$, Days). (**b**) Depth averaged exposure time in winter ($\bar{\theta}$, Days).

The cross-isobath transport plays a pivotal role in establishing hydrodynamic connections between the open ocean and coastal regions, which shows quite significant vertical changes in coastal regions (Figure 2c–f), thus may have different contribution to the water/mass cycle vertically. The $\bar{\theta}_{VD}$ ($\bar{\theta}_{bottom} - \bar{\theta}_{surface}$) serves as a more direct and effective indicator for illustrating the cumulative effects of vertically varying cross-shore motions and displays the clear seasonality.

During summer with prevailing southwest wind forcing, the coastal region experiences substantial surface offshore transport and bottom onshore intrusion (Figure 2c,d). While, despite the prevalence of strong vertically contrasting cross-isobath transport over the shelf, most locally intensified cross-isobath motions do not lead to significant changes in the water exchange rate in the water column. Mainly over the region to the east of Hainan Island and the mouth of Beibu Gulf, the bottom intrusion induces the net increase of the $\bar{\theta}$ (Figure 5a). Over those regions, the bottom water spends approximately 50 days longer time in the NSCS than surface water.

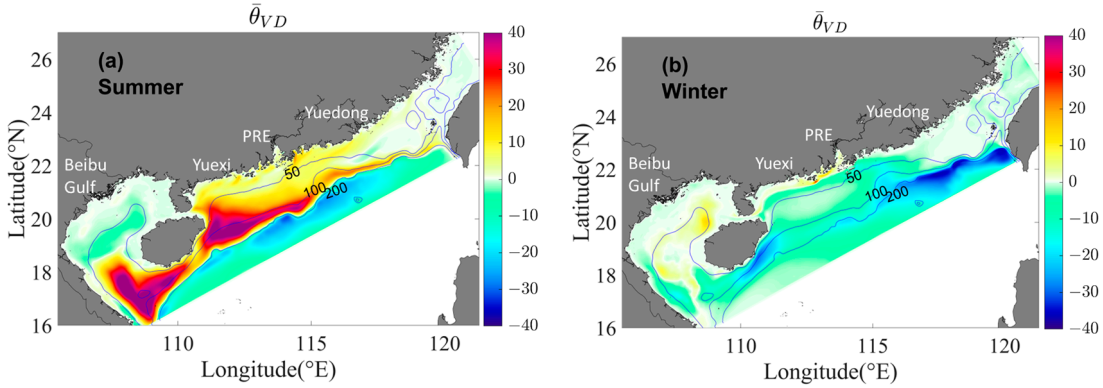

Figure 5. (**a**,**b**) horizontal distribution of $\bar{\theta}_{VD}$ (day) in summer and winter, respectively.

In contrast, during winter with northeast wind forcing and intensified southwest shelf current, it mainly features the surface onshore intrusion and bottom offshore transport, particularly over the southeast of Hainan Island and shelf out of PRE. Thus, the downwelling results in the exchange rate of the bottom water being slightly faster than the surface water with the negative $\bar{\theta}_{VD}$ over the whole shelf NSCS (Figure 5b). However, although the magnitude of the cross-isobath transport is stronger in comparison with the summer, the magnitude of the negative $\bar{\theta}_{VD}$ is much smaller. The large $\bar{\theta}_{VD}$ is only observed near the 200 m isobath and southeast side of Hainan Island.

3.3. Transport Pattern Inferred from $\overline{\theta}_i$

To further check how water moves in the entire NSCS, we examined the time spent in various subdomains before the water finally leaves the NSCS. Based on the topographic and hydrodynamic features, the NSCS was divided into four regions: The Beibu Gulf region (Region A), the semi-closed gulf separated from the vast shelf by Hainan Island. Yuexi region (Region B), the hydrodynamic structure is largely influenced by interaction of the monsoon and Pearl River Plume. PRE region (Region C), where the Pearl River pours fresh water into the NSCS. Yuedong region (Region D), with widen shelf and active Yuedong upwelling (Figure 6). Then, $\overline{\theta}_A - \overline{\theta}_D$, which represents the time of water spent in the four subdomains, was calculated based on Equation (1) by setting δ_ω to 1 in each subdomain [50].

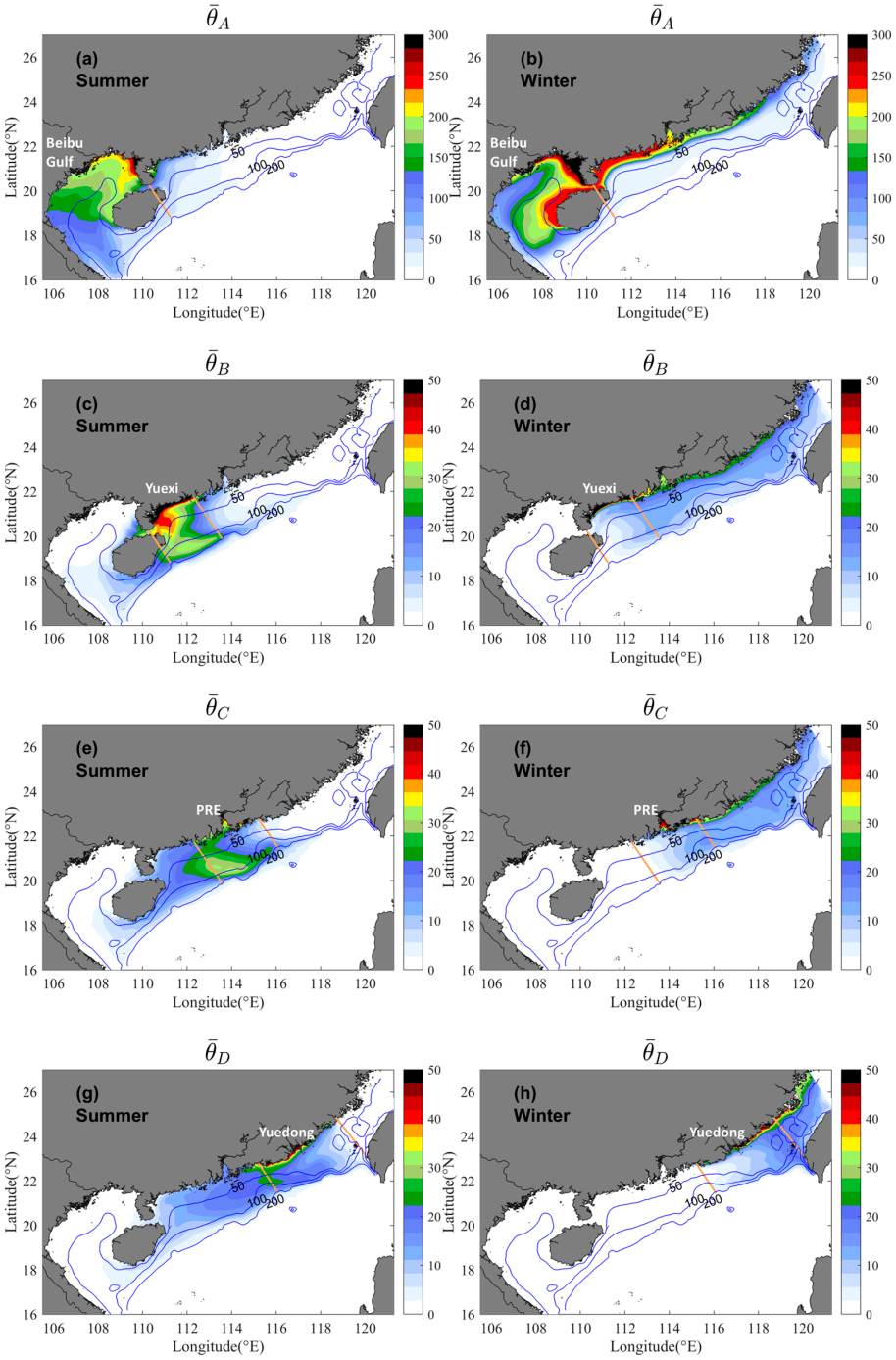

Figure 6. Depth-averaged partial exposure time in summer and winter, respectively ($\overline{\theta}_A - \overline{\theta}_D$, day).

As shown in Figure 6, in the semi-closed Beibu Gulf, the water motions are limited and water exchange rate are relatively low, thus lead to a pronounced increase of $\overline{\theta}_A$, which indicates the time of water stayed in Beibu Gulf is relatively long than the other regions. The $\overline{\theta}_A$ increases from 50 days at the mouth of the gulf to exceed 300 days in the northeast (Figure 6a,b) in both summer and winter, and it has larger contribution to the total $\overline{\theta}$. Outside the Beibu Gulf, in summer, there is an extension of $\overline{\theta}_A$ (~50 days) towards the PRE, potentially indicates a southwestward movement along the coast that against summer wind. Another branch of extension of $\overline{\theta}_A$ expanded along the 100 isobath, indicates the westward transport due to the stable slope current. In winter, high values of $\overline{\theta}_A$ could spread to the coastal areas of Region D, which suggests that, by overriding the shelf current, waters from distant coastal region can arrive the Beibu Gulf.

In Region B-D, the magnitude of the $\overline{\theta}_B \sim \overline{\theta}_D$ is generally shorter than 50 days which represent a much stronger exchanging rate with the open ocean. Spatially, they exhibit a similar pattern, with their magnitudes progressively escalating from the outer shelf towards the inner shelf, and the highest values primarily concentrated along the coastal areas. There is also notably seasonality of $\overline{\theta}_i$ that under the influence of the northeasterly/southwesterly monsoon during summer/winter, non-zero regions of the $\overline{\theta}_B \sim \overline{\theta}_D$ appear in the upstream regions. Besides, it is also noted that during summertime, the $\overline{\theta}_B$ and $\overline{\theta}_C$ have high values on the vicinity of the 100-m isobath line on the outer shelf, although there are quite close to the boundary of NSCS. It suggests a notable onshore exchange of water between the outer shelf and the coastal zones in region B and C during summertime.

Based on the values of $\overline{\theta}_i$ in regions A–D, we could examine the contribution of each $\overline{\theta}_i$ to the overall $\overline{\theta}$ (Figure 7). The x axis and y axis of the bar charts in Figure 7 indicates the different subdomain and the various $\overline{\theta}_i$, respectively. During summer (Figure 7a), generally, it shows substantial contribution of the initial release locations, which means the substance released on the shelf trends to stay in the initial release locations for longer time. Such as the contribution of $\overline{\theta}_A$ exceeds 80% in region A itself. The large contribute of $\overline{\theta}_A$ in Region B and C illustrates a quite strong westward transport, contrary to the prevailing wind and shelf current direction. Even under the northeastward wind forcing and shelf current, the $\overline{\theta}_A$ accounts for approximately 30% and 20% in regions B and C, respectively. In winter (Figure 7b), the strong southwestward shelf current significantly influences the distribution. The $\overline{\theta}_A$ which means the time stay inside the Beibu Gulf, has a significant contribution to all the subdomains, with ratios exceeding 50% in regions B and C and. Even in the region D that quite away from Beibu Gulf, contributions from $\overline{\theta}_A$ reaches 50%. This illustrates the extensive interaction facilitated by shelf circulation, suggesting that the Beibu Gulf marine environment could be affected by the entire NSCS shelf regions.

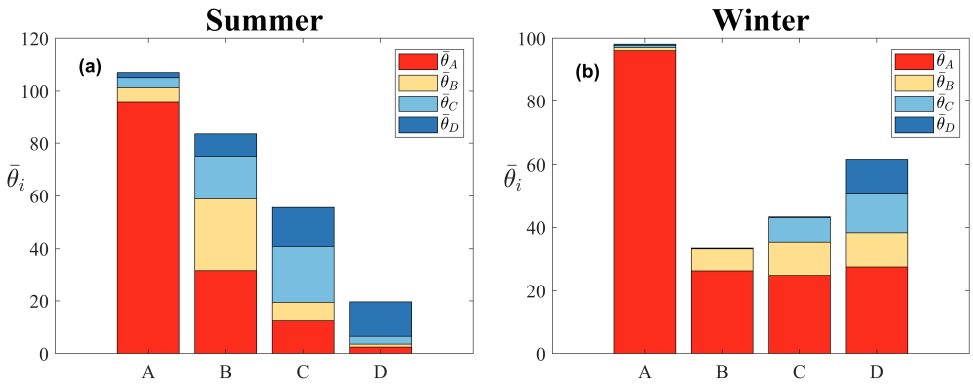

Figure 7. (**a**) Contribution of $\overline{\theta}_A - \overline{\theta}_D$ in different subdomains. Region A is the Beibu Gulf, Region B is the Yuexi Region, Region C is the PRE region, and Region D is the Yuedong Region. (**b**) Same as (**a**) but for winter.

To confirm the westward transport against the wind during summer, we checked the detailed distribution of summer $\overline{\theta}_A$ over the shelf of NSCS. Two branches of extension

of $\overline{\theta}_A$ can be identified (Figure 8a): the first branch extends from the Qiongzhou Strait and eventually reaches to the PRE under the influence of plume, and the second branch expands roughly along100–200 m isobaths which shows the influences of slope current. The Lagrangian tracking provides an alternative perspective for observing the transport structure and connectivity within the NSCS, particularly the westward transport during summer. Figure 8b shows the examples of the summertime trajectories that were released in PRE regions. Along the coast, the expansion of the Pearl River Plume could carry the particles westward, passing through the Yuexi region and finally entering the Beibu Gulf through the Qiongzhou Strait even under the southwest summer wind. Simultaneously, parts of particles released on the vast shelf flow southwestward carried by the slope current (Figure 2a). However, as they approach Hainan Island, some of these particles change direction, move shoreward and eventually become entrapped by the plume. Those particles entered the Beibu Gulf through the Qiongzhou Strait. The remaining particles continue their westward trajectory along the cyclonic slope current and enter the Beibu Gulf from the southern side of Hainan Island. As shown in the previous studies, the ADCP observation and the drifter derived velocity illustrate the southwestward velocity over slope during summer [51,52], which give indirect evidence of this westward transport.

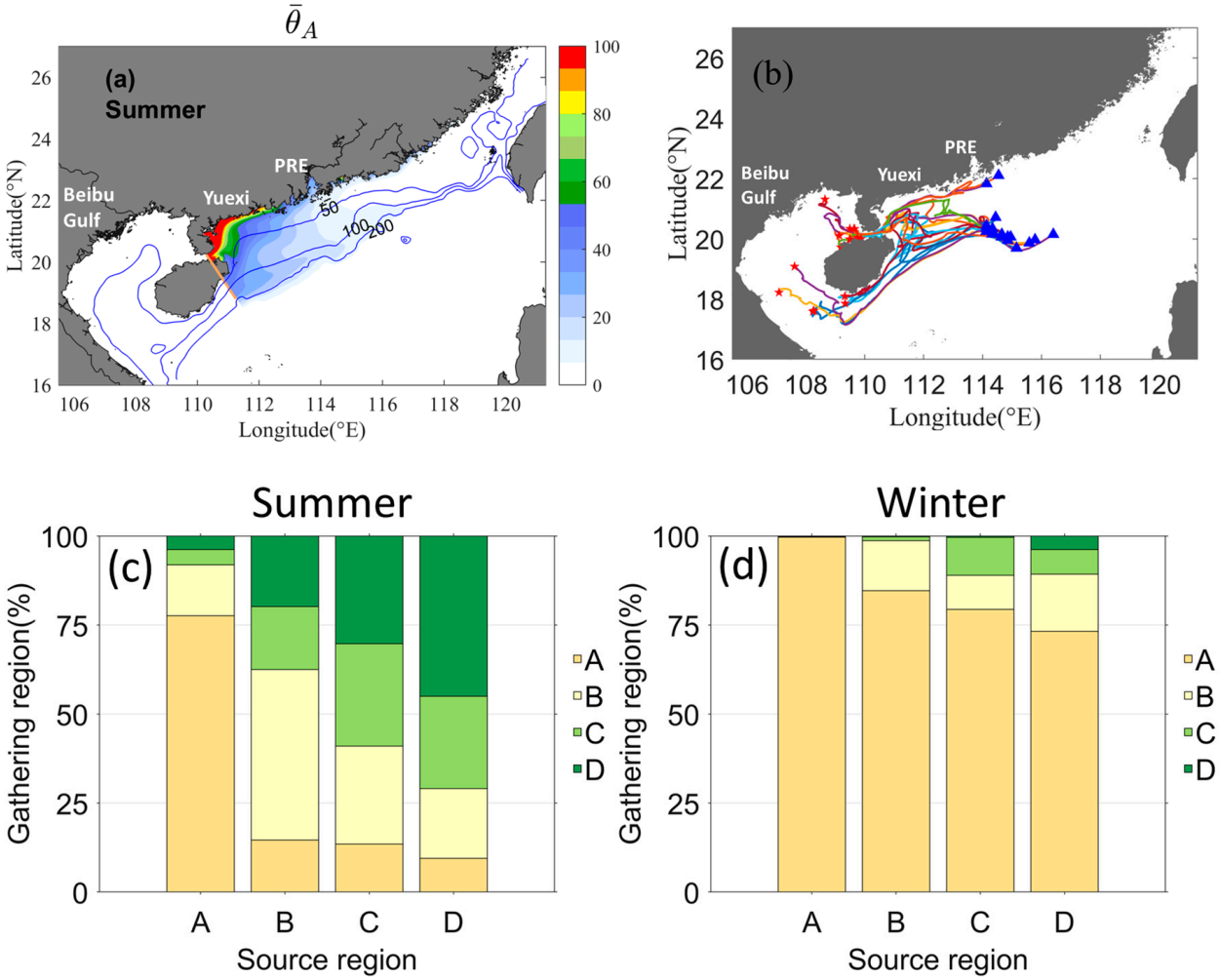

Figure 8. (**a**) Depth-averaged $\overline{\theta}_A$ in summer but ignored the values in Beibu Gulf. (**b**) The trajectories of particles released in the summer. The blue triangles and red stars denote the locations of particles on the 0, 60 days after their release, respectively. (**c**,**d**) Distribution of the particles that released from different regions during summer and winter.

Utilizing the outcomes from Lagrangian tracking, we conducted a statistical analysis of the distribution of particles initially released in different regions (Figure 8c,d). Similar as that obtained from $\overline{\theta}_i$ (Figure 7), during summer with a northeastward shelf current, the particles tend to accumulate in their original release regions and downstream areas. Notably, some particles from Regions B and C ultimately migrate and settle in the Beibu Gulf, following the westward transport pathways depicted in Figure 8b. During the winter, Lagrangian tracking similarly indicates that the majority of particles in the NSCS eventually move to the Beibu Gulf. The distributions of released particles (Figure 8c,d) differ somewhat from the contributions of $\overline{\theta}_i$ (Figure 7) in each subdomain. However, they exhibit a quite similar pattern, suggesting that the results based on exchange times can effectively reveal the predominant transport structures under complicated hydrodynamical processes.

4. Conclusions

In this study, we investigated the spatio-temporal variability of three-dimensional water exchanges under the complex hydrodynamic conditions in NSCS and explored the connectivity among the shelf. Spatially, the annual mean exposure time $\overline{\theta}$ increased from ~30 days over the 200 m isobath to more than 150 days in the coastal region (<50 m), with the largest values occurring at the north of the Beibu Gulf. Seasonally, the water exchange rate shows an immediate response to hydrodynamic conditions. Driven by the monsoon, the strong shelf current triggered a vigorous exchange of water on the northwestern shelf, the horizontal distribution of $\overline{\theta}$ on the board shelf except Beibu Gulf during winter and summer. The distribution of $\overline{\theta}$ in the Beibu Gulf was affected by the seasonally varying cyclonic circulation in the Gulf. However, the largest values in the northeast of the Beibu Gulf were maintained despite of the seasons due to its semi-enclosed nature and restricted water motions. This contrasts with the regions outside the gulf where the water exchange rate is higher, with lower $\overline{\theta}$ suggesting a more dynamic interaction with the open ocean. Vertically, the local vertical contrasting cross-isobath transport did not induce strong vertical changes in net water exchanges, except in several particular regions. Summer months are dominated by substantial surface offshore transport against a counteracting bottom onshore intrusion, while significant positive $\overline{\theta}_{VD}$ (~50 days) mainly occurs east of Hainan Island and at the Beibu Gulf's mouth. During winter, however, the dynamic reverses under the influence of the northeast winds and the intensified southwest shelf current, promoting slightly faster bottom water exchange rates.

Both in summer and winter, the contribution ratio of $\overline{\theta}$ in Beibu Gulf to the NSCS shelf is conspicuous. This area significantly affects adjacent regions, hinting at westward movement against typical currents in summer. Notably, the westward transport is important for water exchange throughout the NSCS, contributing to more than 20% of the time of water exchange over almost the entire shelf, which illustrates the potential influence of the westward spreading of the Pearl River freshwater conjunction with the stable slope current. In winter, the Gulf's influence extends across all regions, with its retention characteristics contributing up to 50% even to distant areas, showing its broad impact on the NSCS's water dynamics throughout the year. It should be noted that the exposure time is a measure of the overall effect of water movement processes, and the research would benefit from including actual measurements. It would enhance our understanding of water exchange rates and transport patterns.

Author Contributions: Conceptualization, T.Z. and Z.C.; Data curation, L.C. and M.L.; Investigation, L.C. and M.L.; Methodology, T.Z.; Supervision, Z.C.; Writing—original draft, L.C.; Writing—review & editing, T.Z. and Z.C. All authors have read and agreed to the published version of the manuscript.

Funding: This work was funded by the Science and Technology Development Fund, Macau SAR (File/Project no. 0093/2020/A2 and SKL-IOTSC-2021-2023; SKL-IoTSC(UM)-2021-2023/ORPF/A20/2022); National Natural Science Foundation of China (NSFC) under Project (42076026), Independent Research Project Program of State Key Laboratory of Tropical Oceanography (LTOZZ2102).

Data Availability Statement: The data used during the current study is available from the corresponding author on reasonable request.

Acknowledgments: This work is supported by CORE which is a joint research centre for ocean research between Laoshan Laboratory and HKUST. This work was performed in part at the SICC, which is supported by the SKL-IOTSC, University of Macau. This work is partly supported by COASTAL-SOS, a project endorsed by UN Decade of Ocean Science for Sustainable Development.

Conflicts of Interest: The authors declare no conflict of interest.

References

1. Cai, Z.; Liu, G.; Liu, Z.; Gan, J. Spatiotemporal variability of water exchanges in the Pearl River Estuary by interactive multiscale currents. *Estuar. Coast. Shelf Sci.* **2022**, *265*, 107730. [CrossRef]
2. Zu, T.; Gan, J. A numerical study of coupled estuary–shelf circulation around the Pearl River Estuary during summer: Responses to variable winds, tides and river discharge. *Deep Sea Res. Part II Top. Stud. Oceanogr.* **2015**, *117*, 53–64. [CrossRef]
3. Lai, W.; Pan, J.; Devlin, A.T. Impact of tides and winds on estuarine circulation in the Pearl River Estuary. *Cont. Shelf Res.* **2018**, *168*, 68–82. [CrossRef]
4. Shang, J.; Sun, J.; Tao, L.; Li, Y.; Nie, Z.; Liu, H.; Chen, R.; Yuan, D. Combined Effect of Tides and Wind on Water Exchange in a Semi-Enclosed Shallow Sea. *Water* **2019**, *11*, 1762. [CrossRef]
5. Hart, J.A.; Phlips, E.J.; Badylak, S.; Dix, N.; Petrinec, K.; Mathews, A.L.; Green, W.; Srifa, A. Phytoplankton biomass and composition in a well-flushed, sub-tropical estuary: The contrasting effects of hydrology, nutrient loads and allochthonous influences. *Mar. Environ. Res.* **2015**, *112 Pt A*, 9–20. [CrossRef]
6. Ryther, J.H.; Dunstan, W.M. Nitrogen, Phosphorus, and Eutrophication in the Coastal Marine Environment. *Science* **1971**, *171*, 1008–1013. [CrossRef] [PubMed]
7. Li, D.; Gan, J.; Hui, C.; Yu, L.; Liu, Z.; Lu, Z.; Kao, S.; Dai, M. Spatiotemporal Development and Dissipation of Hypoxia Induced by Variable Wind-Driven Shelf Circulation off the Pearl River Estuary: Observational and Modeling Studies. *J. Geophys. Res. Oceans* **2021**, *126*, e2020JC016700. [CrossRef]
8. Li, D.; Gan, J.; Hui, R.; Liu, Z.; Yu, L.; Lu, Z.; Dai, M. Vortex and Biogeochemical Dynamics for the Hypoxia Formation Within the Coastal Transition Zone off the Pearl River Estuary. *J. Geophys. Res. Oceans* **2020**, *125*, e2020JC016178. [CrossRef]
9. Shu, Y.; Wang, D.; Feng, M.; Geng, B.; Chen, J.; Yao, J.; Xie, Q.; Liu, Q. The Contribution of Local Wind and Ocean Circulation to the Interannual Variability in Coastal Upwelling Intensity in the Northern South China Sea. *J. Geophys. Res. Oceans* **2018**, *123*, 6766–6778. [CrossRef]
10. Gan, J.; Cheung, A.; Guo, X.; Li, L. Intensified upwelling over a widened shelf in the northeastern South China Sea. *J. Geophys. Res.* **2009**, *114*, C09019. [CrossRef]
11. Ou, S.; Zhang, H.; Wang, D.-X. Dynamics of the buoyant plume off the Pearl River Estuary in summer. *Environ. Fluid Mech.* **2009**, *9*, 471–492. [CrossRef]
12. Pan, J.; Gu, Y.; Wang, D. Observations and numerical modeling of the Pearl River plume in summer season. *J. Geophys. Res. Oceans* **2014**, *119*, 2480–2500. [CrossRef]
13. Shi, W.; Huang, Z.; Hu, J. Using TPI to Map Spatial and Temporal Variations of Significant Coastal Upwelling in the Northern South China Sea. *Remote Sens.* **2021**, *13*, 1065. [CrossRef]
14. Jiang, R.; Wang, Y.-S. Modeling the ecosystem response to summer coastal upwelling in the northern South China Sea. *Oceanologia* **2018**, *60*, 32–51. [CrossRef]
15. Dong, L.; Su, J.; Ah Wong, L.; Cao, Z.; Chen, J.-C. Seasonal variation and dynamics of the Pearl River plume. *Cont. Shelf Res.* **2004**, *24*, 1761–1777. [CrossRef]
16. Gao, J.; Shi, M.; Chen, B.; Guo, P.; Zhao, D. Responses of the circulation and water mass in the Beibu Gulf to the seasonal forcing regimes. *Acta Oceanol. Sin.* **2014**, *33*, 1–11. [CrossRef]
17. Quan, Q.; Liu, Z.; Sun, S.; Cai, Z.; Yang, Y.; Jin, G.; Li, Z.; Liang, X.S. Influence of the Kuroshio Intrusion on Deep Flow Intraseasonal Variability in the Northern South China Sea. *J. Geophys. Res. Oceans* **2021**, *126*, e2021JC017429. [CrossRef]
18. Gao, X.; Zhao, G.; Zhang, C.; Wang, Y. Modeling the exposure time in a tidal system: The impacts of external domain, tidal range, and inflows. *Environ. Sci. Pollut. Res.* **2018**, *25*, 11128–11142. [CrossRef]
19. Cucco, A.; Umgiesser, G. Modeling the Venice Lagoon residence time. *Ecol. Model.* **2006**, *193*, 34–51. [CrossRef]
20. Du, J.; Shen, J. Water residence time in Chesapeake Bay for 1980–2012. *J. Mar. Syst.* **2016**, *164*, 101–111. [CrossRef]
21. Liu, Z.; Wei, H.; Liu, G.; Zhang, J. Simulation of water exchange in Jiaozhou Bay by average residence time approach. *Estuar. Coast. Shelf Sci.* **2004**, *61*, 25–35. [CrossRef]
22. Deleersnijder, E.; Campin, J.-M.; Delhez, E.J. The concept of age in marine modelling: I. Theory and preliminary model results. *J. Mar. Syst.* **2001**, *28*, 229–267. [CrossRef]
23. Ren, Y.; Lin, B.; Sun, J.; Pan, S. Predicting water age distribution in the Pearl River Estuary using a three-dimensional model. *J. Mar. Syst.* **2014**, *139*, 276–287. [CrossRef]
24. Cui, L.; Cai, Z.; Liu, Z. Water exchange and transport pathways in estuary-shelf region of Pearl River Estuary under multiple forcings. *Cont. Shelf Res.* **2023**, *266*, 105099. [CrossRef]

25. Zhang, H.; Cheng, W.; Chen, Y.; Shi, Z.; Gong, W.; Liu, S. Importance of large-scale coastal circulation on bay-shelf exchange and residence time in a subtropical embayment, the northern South China Sea. *Ocean Coast. Manag.* **2019**, *168*, 72–89. [CrossRef]
26. Liu, Z.; Zu, T.; Gan, J. Dynamics of cross-shelf water exchanges off Pearl River Estuary in summer. *Prog. Oceanogr.* **2020**, *189*, 102465. [CrossRef]
27. Shchepetkin, A.F.; McWilliams, J.C. The regional oceanic modeling system (ROMS): A split-explicit, free-surface, topography-following-coordinate oceanic model. *Ocean Model.* **2005**, *9*, 347–404. [CrossRef]
28. Song, Y.; Haidvogel, D. A semi-implicit ocean circulation model using a generalized topography-following coordinate system. *J. Comput. Phys.* **1994**, *115*, 228–244. [CrossRef]
29. Mellor, G.L.; Yamada, T. Development of a turbulence closure model for geophysical fluid problems. *Rev. Geophys.* **1982**, *20*, 851–875. [CrossRef]
30. Egbert, G.D.; Erofeeva, S.Y. Efficient inverse modeling of barotropic ocean tides. *J. Atmos. Ocean. Technol.* **2002**, *19*, 183–204. [CrossRef]
31. Zu, T.; Gan, J.; Erofeeva, S.Y. Numerical study of the tide and tidal dynamics in the South China Sea. *Deep Sea Res. Part I Oceanogr. Res. Pap.* **2008**, *55*, 137–154. [CrossRef]
32. Deng, Y.; Liu, Z.; Zu, T.; Hu, J.; Gan, J.; Lin, Y.; Li, Z.; Quan, Q.; Cai, Z. Climatic Controls on the Interannual Variability of Shelf Circulation in the Northern South China Sea. *J. Geophys. Res. Oceans* **2022**, *127*, e2022JC018419. [CrossRef]
33. Brauwere, A.d.; de Brye, B.; Blaise, S.; Deleersnijder, E. Residence time, exposure time and connectivity in the Scheldt Estuary. *J. Mar. Syst.* **2011**, *84*, 85–95. [CrossRef]
34. Delhez, É.J.M.; Deleersnijder, É. The boundary layer of the residence time field. *Ocean Dyn.* **2006**, *56*, 139–150. [CrossRef]
35. Delhez, É.J.M.; Heemink, A.W.; Deleersnijder, E. Residence time in a semi-enclosed domain from the solution of an adjoint problem. *Estuar. Coast. Shelf Sci.* **2004**, *61*, 691–702. [CrossRef]
36. Zhang, D.Q.; Tan, S.K.; Gersberg, R.M. Municipal solid waste management in China: Status, problems and challenges. *J. Environ. Manag.* **2010**, *91*, 1623–1633. [CrossRef] [PubMed]
37. North, E.W.; Adams, E.E.; Schlag, Z.; Sherwood, C.R.; He, R.; Hyun, K.H.; Socolofsky, S.A. Simulating Oil Droplet Dispersal from the Deepwater Horizon Spill with a Lagrangian Approach. In *Monitoring and Modeling the Deepwater Horizon Oil Spill: A Record-Breaking Enterprise*; American Geophysical Union: Washington, DC, USA, 2011; pp. 217–226. [CrossRef]
38. Chu, N.; Liu, G.; Xu, J.; Yao, P.; Du, Y.; Liu, Z.; Cai, Z. Hydrodynamical transport structure and lagrangian connectivity of circulations in the Pearl River Estuary. *Front. Mar. Sci.* **2022**, *9*, 996551. [CrossRef]
39. Liang, J.-H.; Liu, J.; Benfield, M.; Justic, D.; Holstein, D.; Liu, B.; Hetland, R.; Kobashi, D.; Dong, C.; Dong, W. Including the effects of subsurface currents on buoyant particles in Lagrangian particle tracking models: Model development and its application to the study of riverborne plastics over the Louisiana/Texas shelf. *Ocean Model.* **2021**, *167*, 101879. [CrossRef]
40. North, E.; Hood, R.; Chao, S.-Y.; Sanford, L. Using a random displacement model to simulate turbulent particle motion in a baroclinic frontal zone: A new implementation scheme and model performance tests. *J. Mar. Syst.* **2006**, *60*, 365–380. [CrossRef]
41. Zhong, L.J.; Li, M. Tidal energy fluxes and dissipation in the Chesapeake Bay. *Cont. Shelf Res.* **2006**, *26*, 752–770. [CrossRef]
42. Shu, Y.; Wang, Q.; Zu, T. Progress on shelf and slope circulation in the northern South China Sea. *Sci. China Earth Sci.* **2018**, *61*, 560–571. [CrossRef]
43. Shu, Y.; Chen, J.; Yao, J.; Pan, J.; Wang, W.; Mao, H.; Wang, D. Effects of the Pearl River plume on the vertical structure of coastal currents in the Northern South China Sea during summer 2008. *Ocean Dyn.* **2014**, *64*, 1743–1752. [CrossRef]
44. Gan, J.; Li, L.; Wang, D.; Guo, X. Interaction of a river plume with coastal upwelling in the northeastern South China Sea. *Cont. Shelf Res.* **2009**, *29*, 728–740. [CrossRef]
45. Gan, J.; Wang, J.; Liang, L.; Li, L.; Guo, X. A modeling study of the formation, maintenance, and relaxation of upwelling circulation on the Northeastern South China Sea shelf. *Deep Sea Res. Part II Top. Stud. Oceanogr.* **2015**, *117*, 41–52. [CrossRef]
46. Brink, K.H. Cross-Shelf Exchange. *Annu. Rev. Mar. Sci.* **2016**, *8*, 59–78. [CrossRef] [PubMed]
47. Gao, J.; Chen, B.; Shi, M. Summer circulation structure and formation mechanism in the Beibu Gulf. *Sci. China Earth Sci.* **2014**, *58*, 286–299. [CrossRef]
48. Wu, D.; Wang, Y.; Lin, X.; Yang, J. On the mechanism of the cyclonic circulation in the Gulf of Tonkin in the summer. *J. Geophys. Res. Atmos.* **2008**, *113*, C09029. [CrossRef]
49. Gao, J.; Wu, G.; Ya, H. Review of the circulation in the Beibu Gulf, South China Sea. *Cont. Shelf Res.* **2017**, *138*, 106–119. [CrossRef]
50. Lin, L.; Liu, Z. Partial residence times: Determining residence time composition in different subregions. *Ocean Dyn.* **2019**, *69*, 1023–1036. [CrossRef]
51. Fang, W.; Guo, P.; Liu, C.; Fang, G.; Li, S. Observed sub-inertial current variability and volume transport over the continental shelf in the northern South China Sea. *Estuar. Coast. Shelf Sci.* **2015**, *157*, 19–31. [CrossRef]
52. Huang, G.; Zhan, H.; He, Q.; Wei, X.; Li, B. A Lagrangian study of the near-surface intrusion of Pacific water into the South China Sea. *Acta Oceanol. Sin.* **2021**, *40*, 15–30. [CrossRef]